

Article

Theoretical Simulation of the High-Order Harmonic Generated from Neon Atom Irradiated by the Intense Laser Pulse

Siqi Wei ^{1,2}, Yun Pan ^{3,*}, Yue Qiao ^{1,2}, Shushan Zhou ⁴, Haiying Yuan ^{1,2,5}, Jun Wang ^{1,2,*} , Fuming Guo ^{1,2,*} and Yujun Yang ^{1,2}¹ Institute of Atomic and Molecular Physics, Jilin University, Changchun 130012, China² Jilin Provincial Key Laboratory of Applied Atomic and Molecular Spectroscopy, Jilin University, Changchun 130012, China³ Department of Preparatory Course, Shenyang Institute of Engineering, Shenyang 110136, China⁴ School of Physics and Electronic Technology, Liaoning Normal University, Dalian 116029, China⁵ College of Physics, Jilin University, Changchun 130012, China

* Correspondence: panyun@sie.edu.cn (Y.P.); wangjun86@jlu.edu.cn (J.W.); guofm@jlu.edu.cn (F.G.)

Abstract: Based on the strong field approximation theory and numerical solution of Maxwell's propagation equations, the high-order harmonic is generated from a neon (Ne) atom irradiated by a high-intensity laser pulse whose central wavelength is 800 nm. In the harmonic spectrum, it is found that in addition to the odd harmonics of the driving laser, a new frequency peak appeared. By examining the time-dependent behavior of the driving laser, it is found that the symmetry of the laser field is broken. We demonstrated that these new spectrum peaks are caused by the intensity reduction and frequency blue shift of the high-intensity laser during propagation. Our results reveal that it is feasible to modulate the harmonics of the specific energy to produce high-intensity harmonic emission by changing the gas density and the position of the gas medium interacting with the laser pulse.

Keywords: high-order harmonic generation; phase matching

Citation: Wei, S.; Pan, Y.; Qiao, Y.; Zhou, S.; Yuan, H.; Wang, J.; Guo, F.; Yang, Y. Theoretical Simulation of the High-Order Harmonic Generated from Neon Atom Irradiated by the Intense Laser Pulse. *Symmetry* **2023**, *15*, 636. <https://doi.org/10.3390/sym15030636>

Academic Editors: Shicheng Jiang and Jigen Chen

Received: 29 December 2022

Revised: 18 February 2023

Accepted: 24 February 2023

Published: 3 March 2023



Copyright: © 2023 by the authors. Licensee MDPI, Basel, Switzerland. This article is an open access article distributed under the terms and conditions of the Creative Commons Attribution (CC BY) license (<https://creativecommons.org/licenses/by/4.0/>).

1. Introduction

Many plentiful nonlinear phenomena [1–4] can be generated by ultrafast strong laser interactions with atoms [5–9], molecules [10–13], and solids [14–20] including coherent high energy harmonic emission, which can be applied to produce coherent tabletop light sources of the tunable extreme ultraviolet and soft X-ray region [21–27], as well as in coherent diffraction imaging, ultrafast holography, and ultra-high time-resolved measurements [28–36]. Due to the spatial symmetry, only odd harmonics can be observed in the harmonics generated by atoms irradiated by the laser pulse. In the decades since it was first detected experimentally, the phenomena of high-order harmonic generation (HHG) have progressed significantly. On the one hand, using a 4 μm mid-infrared driven laser to interact with helium atoms at high pressure, it was experimentally observed that HHG exceeds 5000 orders of magnitude and harmonic energies up to 1.6 keV [37]. On the other hand, the supercontinuous high-order harmonic emission spectrum obtained by the mid-infrared laser produces ultrashort pulses of 43 attoseconds (as) [38]. However, the efficiency of harmonics generated remains relatively low, which restricts the further application of HHG. To address this issue, more in-depth research has been conducted.

The generation of gaseous harmonics can be broadly divided into two parts: the response from a single atom to the driving field and the coherence of harmonics generated by different atoms of the gas system (propagation effect). Numerous schemes to improve the harmonic emission efficiency have been proposed for the single-atom response. In order to improve harmonic efficiency, in 1994, Watanabe et al. [39] experimented with the titanium sapphire laser and triple frequency two-color field and found that adding a

third harmonic with an intensity of only 10% of the fundamental frequency laser intensity can increase ion yield by 7 times. The suprathreshold ionization peak caused by the third harmonic disappears in the photoelectron spectrum when the two-color superposition is achieved, forming a continuous spectrum, indicating that the coherent control of the two-color field is successfully achieved under tunneling conditions, and the results show that the harmonic efficiency of the platform region is increased by an order of magnitude. Tong and Rundquist et al. proposed to optimize the laser field waveform by the two-color field or the multi-color field and then control the electron trajectory during harmonic emission [40]. Lan et al. proposed an attosecond ionization gate composed of a two-color laser field to modulate the generation of electron wave packets, thereby effectively improving the harmonic yield [41]. Hong et al. significantly enhanced the yield of the continuous harmonic spectrum through the field [42]. Luo et al. used UV pulses to assist ionization in enhancing the quantum paths affecting the harmonics, thereby effectively improving the intensity of the supercontinuum spectrum [43]. However, many of these approaches fail to significantly improve efficiency when considering propagation effects, especially for different gas pressures and driving laser focusing conditions, where the same laser setup produces considerably different results because the plasma generated by the interaction of the driving laser with the atomic gas target no longer maintains the characteristics of the driving field for different gas pressures and driving laser parameters. In comparison, the harmonic intensity of the harmonics cannot be effectively regulated due to different phase-matching conditions of harmonic generation and gas absorption and scattering processes. Hence, the harmonic efficiency is usually regulated from the collective effect of the harmonic propagation.

The phase matching [44–47] requirements for harmonic production must be improved to maximize the harmonic efficiency from a macroscopic perspective. Changing gas density to achieve harmonic tuning is typically a direct method. For example, earlier studies by Chen et al. observed that at lower laser energies, the intensity of harmonic emission can be steadily enhanced as the gas density of nitrogen 7th to 17th harmonics increase [48]. Based on the interaction of Ne atom gas with 1200 nm few-cycle mid-infrared laser pulses, Pan et al. found that the quantum trajectory of harmonic generation can be controlled in the mid-infrared case, which in turn produces isolated attosecond pulses [49]. Since the harmonic efficiency declines with the increasing wavelength of the driving laser pulse, the aforementioned research could not successfully modulate the harmonic emission.

When a gas medium is ionized, the refractive index changes, causing the laser transmitted in the medium to produce spectral modulation, also known as self-phase modulation (SPM). The blue-shift phenomenon of harmonics is the result of self-phase modulation. Wahlström et al. studied the blue shift phenomenon of Xe and Ar high-order harmonic radiation generated by the pulse valve [50]. According to Kan et al., high harmonic generation in ionizing atomic gases ought to be accompanied by an intensity-dependent harmonic phase, which in a practical experimental setting would lead to a clearly visible blue shift and line splitting in the midplateau harmonics. Subsequently, the non-adiabatic blue shift of the high-order harmonic from Ar was first experimentally discovered by Shin [51] et al. By adjusting the respective positions of the pulse valve and the laser focus [52], Altucci et al. were able to continuously tune harmonic radiation in the range of less than 20 nm. In addition, the harmonic blueshift phenomena will be brought on by the non-adiabatic effect produced by the quickly growing laser electric field [53]. Lu et al. experimentally investigated the spectrum blueshift properties of Ne phase-matched higher-order harmonics. When laser pulses are delivered across a gas ionization medium, the produced self-phase modulation (SPM) causes harmonics to turn blue [54]. Furthermore, pulse valve systems make it challenging to determine the gas density with accuracy. High gas density can be attained inside the gas box much more simply than using pulse valves. Additionally, the gas box can expand the laser-gas interaction region, boost harmonic photon flux, and make it easier to capture powerful high-order harmonic radiation. Reitze et al.'s use of an evolutionary strategy algorithm in combination with a shaping laser pulse allowed them

to tune the harmonic wavelength of Ar in the gas box and increase the harmonic photon flux [55]. Nefedova et al. explained the microscopic effect of spectral movement of Ne and He higher harmonic radiation generated by pulse valves. Moreover, through experimental data, it was discovered that when the contribution of long electron trajectories is less than 10%, the contribution of higher harmonics to spectral motion cannot be ignored by the atomic dipole phase [56].

In this study, we focused on the harmonic emission of the Ne atoms caused by a high-intensity driving pulse of 800 nm. In this case, new energy peaks appear in the harmonic emission spectrum under this situation. By examining the driving laser field and the harmonic propagation process, it is demonstrated that the cause of this phenomenon is that atoms rapidly ionize to form plasma under the action of a high-intensity driving laser. As the fundamental drive field strength decreases, the frequency shifts to blue. Based on this method, the gas density may be tuned to improve the generation of higher-intensity harmonic emissions. The organization of this paper is as follows. We first propose the theoretical model and computational scheme selected for the study. Next, the results of the numerical calculations are given and discussed in detail. The results of the study are summarized at the end of the paper.

2. Materials and Methods

In order to study the process of harmonic generation by the interaction between an intense laser field and atomic gas, we need to calculate the single-atom response of atoms and the propagation equation of the laser field.

A. Single-atom response

In order to resolve the time-dependent Schrödinger equation for atoms in low-frequency laser beams, Lewenstein et al. devised an analytical theory in 1994. The three-step model provided by Corkum et al. provides a traditional justification for the hypothesis. The “Lewenstein model” or “strong field approximation model” are common names for this theory (SFA). We applied the strong-field theory by Lewenstein to calculate the single-atom response under the action of the laser field [57]. The time-dependent dipole moment of the atom under the action of the laser field is expressed as:

$$D(t) = -i \int_0^\infty d\tau \left[\frac{\pi}{\varepsilon + i\tau/2} \right]^{3/2} d_x^* (\vec{p}_{st} + \vec{A}(t)) g^*(t) \exp[-iS(\vec{p}_{st}, t, \tau)] \times E(t - \tau) d_x (\vec{p}_{st} + \vec{A}(t - \tau)) g(t - \tau) + c.c. \quad (1)$$

where, $\vec{p}_{st} = -\frac{1}{\tau} \int_{t-\tau}^t \vec{A}(t') dt'$, $S(\vec{p}_{st}, t, \tau) = I_p \tau - \frac{1}{2} \vec{p}_{st}^2 \tau + \frac{1}{2} \int_{t-\tau}^t \vec{A}^2(t') dt'$ is the asymptotic momentum and a semi-classical action quantity. $E(t)$ is the laser field. $A(t)$ is the vector potential corresponding to the atom in the theoretical simulation. $g(t) = \exp\left(-\int_0^t \frac{\gamma(t')}{2} dt'\right)$ is the ground state amplitude in numerical simulations. $\gamma(t')$ is the ionization rate during the experiment.

The equation for the high-order harmonic spectrum is

$$P_{(w)} = |d_q(w)|^2 \quad (2)$$

After the Fourier transform, the dipole acceleration becomes

$$d_q(\omega) = \frac{1}{\sqrt{2\pi}} \int_{-\infty}^{\infty} D(t) \exp(-iq\omega t) dt \quad (3)$$

where ω is the central frequency of the laser pulse while q represents the harmonic order, respectively.

B. Propagation of fundamental and harmonic fields.

We consider the spatial distribution of the electric field driving the laser as: $E_1(r, z', t') = \text{Re} [E_{\text{gau}}(r, z')A(r, z', t')e^{-i(\omega_0 t' + \phi_{CE})}]$ where the equations below are valid:

$$\begin{aligned}
 E_{\text{gau}}(r, z') &= \frac{bE_0}{b + 2iz'} \exp\left(-\frac{kr^2}{b + 2iz'}\right) \\
 A(r, z', t') &= \exp\left[-(2 \ln 2) \frac{(t' - \phi_{\text{laser}}(r, z')/\omega_0)^2}{\tau_\omega^2}\right] \\
 \phi_{\text{laser}}(r, z') &= -\tan^{-1}\left(\frac{2z'}{b}\right) + \frac{2kr^2z'}{b^2 + 4z'^2}
 \end{aligned}
 \tag{4}$$

To simulate the collective response of the macroscopic gas, the propagation of the fundamental frequency laser field in the medium under the cylindrical coordinates can be expressed by Maxwell’s propagation equations and solved numerically by the Crank–Nicolson’s method [58–60]:

$$\nabla^2 E_1(r, z, t) - \frac{1}{c^2} \frac{\partial^2 E_1(r, z, t)}{\partial t^2} = \mu_0 \frac{\partial J_{\text{abs}}(r, z, t)}{\partial t} + \frac{\omega_0^2}{c^2} (1 - \eta_{\text{eff}}^2) E_1(r, z, t)
 \tag{5}$$

$$\nabla^2 E_h(r, z, t) - \frac{1}{c^2} \frac{\partial^2 E_h(r, z, t)}{\partial t^2} = \mu_0 \frac{\partial^2 P(r, z, t)}{\partial t^2}
 \tag{6}$$

in Equations (5) and (6), $E_1(r, z, t)$ is the fundamental frequency laser pulse field, $E_h(r, z, t)$ is the harmonic field, z is the direction of laser propagation, and r is the radial distance, respectively.

The effective refractive index of the medium for the experimental conditions is:

$$\eta_{\text{eff}}(r, z, t) = \eta_0(r, z, t) + \eta_2 I(r, z, t) - \frac{\omega_p^2(r, z, t)}{2\omega_0^2}
 \tag{7}$$

The first term $\eta_0 = 1 + \delta_1 - i\beta_1$ on the right of the equation contains the refraction δ_1 and absorption effects of the neutral atom β_1 ; the second term is the Kerr effect term, which is limited by the intensity of the laser $I(r, z, t)$; and the third term is based on the free electron. The plasma frequency is $\omega_p(r, z, t) = [e^2 n_e(r, z, t) / (\epsilon_0 m_e)]^{1/2}$, with the mass of the electron represented by m_e , the charge of the electron by e , and the density of the free electron by $n_e(r, z, t)$.

J_{abs} in Equation (5) was the absorption term for the dissociated medium.

$$J_{\text{abs}}(r, z, t) = \frac{\gamma(r, z, t)(n_0 - n_e(r, z, t))I_p E_1(r, z, t)}{|E_1(r, z, t)|^2}
 \tag{8}$$

where $\gamma(r, z, t)$ is ionization rate. $P(r, z, t)$ is the polarization term, which depending on the laser field $E_1(r, z, t)$.

C. Far-field harmonics

Near-field harmonics, which are harmonics that are released in the exit plane of a gaseous medium, propagate further in a vacuum before being picked up by the spectrometer. Before reaching the detector, harmonics may go through slits, iris, or pinholes, or they may reflect off of mirrors or other sophisticated optical devices (called far-field harmonics). The far-field harmonics are obtained through subjecting the near-field harmonics to the Hankel transform [61–63]:

$$E_h^f(r_f, z_f, \omega) = -ik \int \frac{\tilde{E}_h(r, z', \omega)}{z_f - z'} J_0\left(\frac{kr r_f}{z_f - z'}\right) \exp\left[\frac{ik(r^2 + r_f^2)}{2(z_f - z')}\right] r dr
 \tag{9}$$

where J_0 is the zero-order Bessel function, z_f is the distance away from the laser focus position, r_f is the transverse coordinate in the far field, and $k = \omega/c$ is the wave vector k .

3. Results and Analysis

We used an 800 nm driving laser with a focusing peak intensity of 10^{15} W/cm², a pulse duration of 30 fs, and a laser beam waist of 25 μ m. The Neon atom gas target was located on the laser focus with a medium length of 1 mm. Figure 1a depicts the corresponding harmonic emission spectrum. As can be seen from Figure 1a, the generated near-field harmonics exhibit a clear platform structure. The cut-off energy of the harmonic spectrum is approximately the 80th harmonic, which is substantially lower than the cut-off energy (135th harmonic) of the single-atom response at this intensity. The harmonic spectrum still exhibits odd-order harmonic properties below the threshold value. However, as harmonic energy rises, more numerous spectral patterns become visible. It should be noted that in addition to odd harmonic peaks, new spectral peaks can be seen. As the harmonic order grows, the energy location of the new spectral lines gradually drifts away from the harmonic peak energy position, which is also shown in the inset of Figure 1a. When the harmonic energy increases further, the spectral structure of harmonic emission becomes increasingly complex, showing a multimodal mode. It has been found that the multi-peak patterns during the propagation are caused by the changes in the waveform driving the laser, which we will explore in detail. In the far-field case, the new spectral peak characteristics can be observed more clearly, as depicted in Figure 1b. Far-field harmonics exhibit two characteristics, as seen in Figure 1b. Odd-order harmonics have a higher emission intensity and a smaller divergence angle. Near the odd harmonic peak, the harmonic emission's width is narrower while its divergence angle is larger.

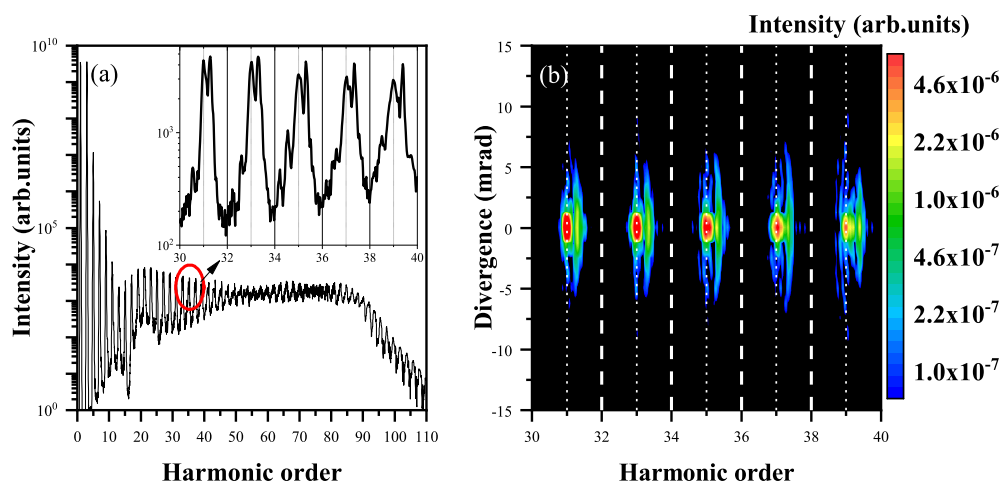


Figure 1. (a) The near-field HHG spectra generated by an intense laser pulse at 800 nm. (b) The spatial distribution of the divergence angles of the far-field harmonics at different positions along and off the axis.

To better understand the nature of these harmonics, we estimated the variations in the harmonic emission spectrum along the direction of harmonic propagation, as shown in Figure 2. The graph shows that with the increase in z , the spectral intensity of odd harmonic emission reaches the maximum value when $z = -0.2$ mm. When z increases further, the harmonic intensity begins to decrease, while a new spectral peak arises near the odd-order harmonics at $z = 0.1$ mm, the strength of this peak grows with the propagation distance. It should be noted that with a subsequent increase in distance, the intensity of odd harmonics remains constant.

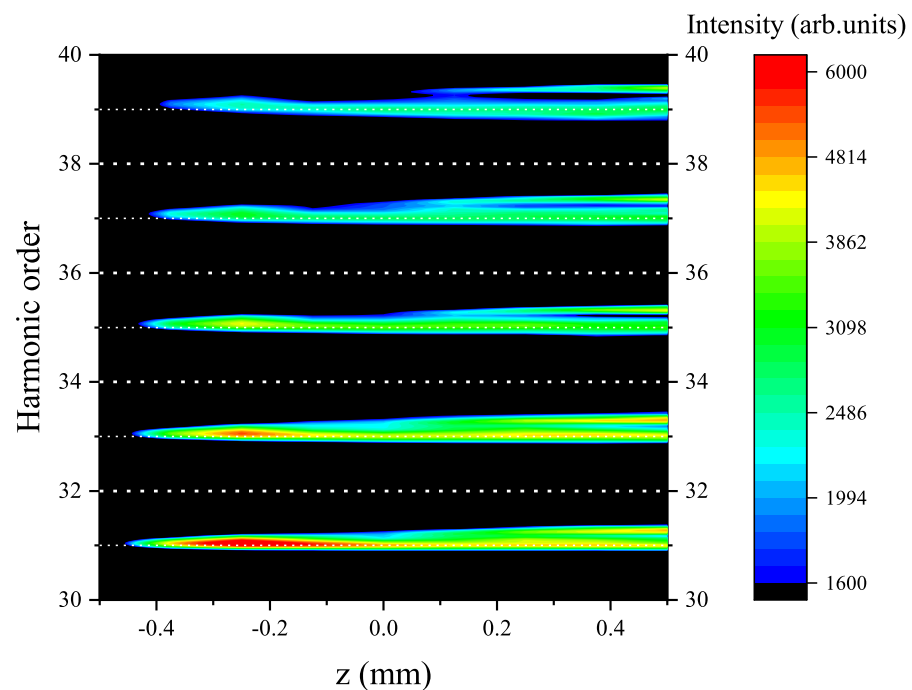


Figure 2. The relationship between the propagation position and the harmonic intensity distribution of various harmonic orders.

Considering that harmonic emission is a driven laser field's nonlinear reaction to an atom, in order to study how the driven laser field changes with propagation position, we further explored the variation of the driven laser field, as shown in Figure 3a. The diagram displays the variation of the driving laser intensity at different spatial positions r with the propagation position z . It can be seen from the figure that as the driving laser gradually diffuses towards the focus, the intensity of the driving laser does not increase. Instead, it shows a tendency to decay rapidly. When $z = 0$ is reached, the intensity of the driven field decreases slowly until the end of the laser and remains at a lower amplitude. This phenomenon was caused by the rapid ionization of atoms caused by high-intensity laser pulses, which causes the plasma to form in the gas at low pressure [64–66] and defocus the driving laser [67,68]. In this way, after the medium's effective refractive index and intense phase modulation change rapidly, the intensity of the driving laser decreases [69]. For a more detailed view of the changes in the driving laser, Figure 3b presents the change in intensity with r for the positions $z = -0.5$ mm (black solid line) and $z = 0.5$ mm (red dotted line), respectively. The diagram makes it evident that, at the $z = 0.5$ mm location, the field's primary energy is concentrated close to the axis. Furthermore, the laser intensity rapidly drops as the distance from the axis increases. At the position of $z = 0.5$ mm, not only does the axial intensity decrease rapidly, but the intensity changes slowly with the change of r . There is still a large intensity distribution at the position far from the optical axis.

In addition to the intensity of the driving laser, the more critical factor affecting the harmonic generation is the waveform of the driving laser. In Figure 4, we display the change in the time-dependent amplitude of the driving laser field at several spatial locations to analyze this effect. From Figure 4a, it can be clearly observed that the peak amplitude of the driving laser field varies significantly from $z = -0.5$ mm to $z = 0$ while the peak amplitude changes negligibly from $z = 0$ to $z = 0.5$ mm. The time-dependent amplitude change characteristics of the laser field also show different behaviors, with a bit of change in the laser field along the rising edge of the laser pulse and a significant change in the laser field close to the peak of the laser pulse, as seen in Figure 4b, where the central wavelength of the driving optical field also moves toward the high-energy zone.

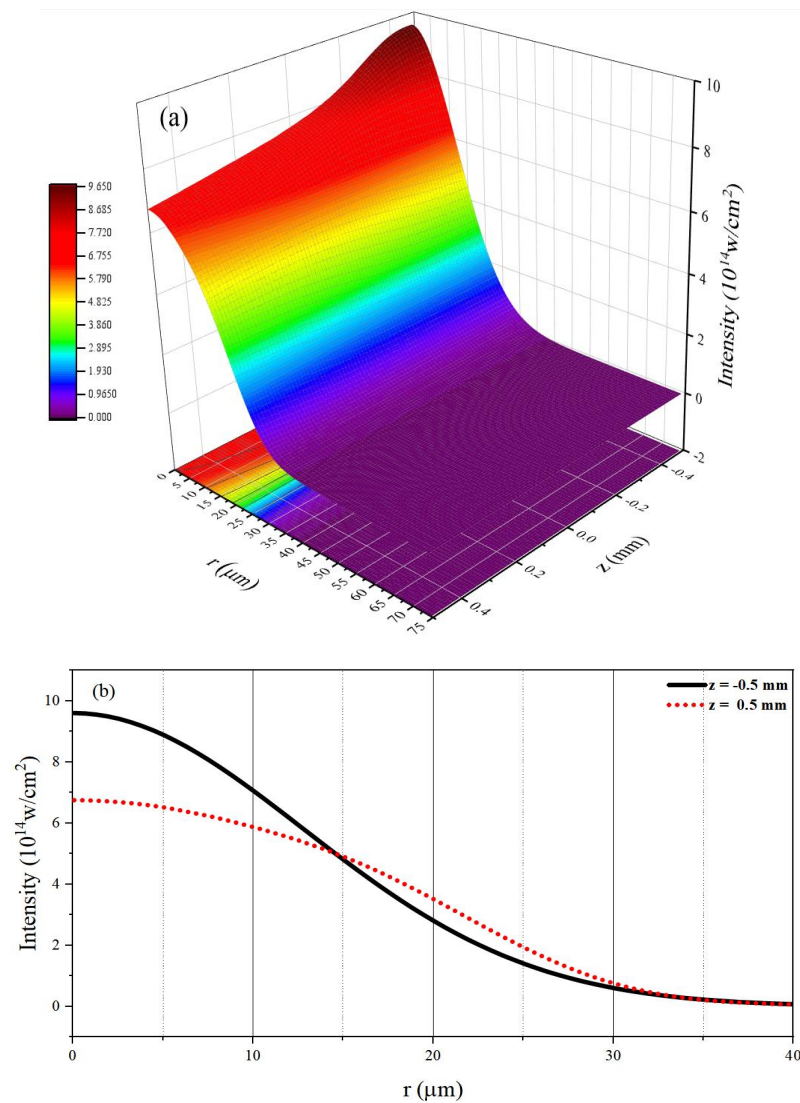


Figure 3. (a) Spatial evolution of the laser field. (b) Radial distribution of the electric field intensity before (black solid line) and after (red dotted line) the propagation.

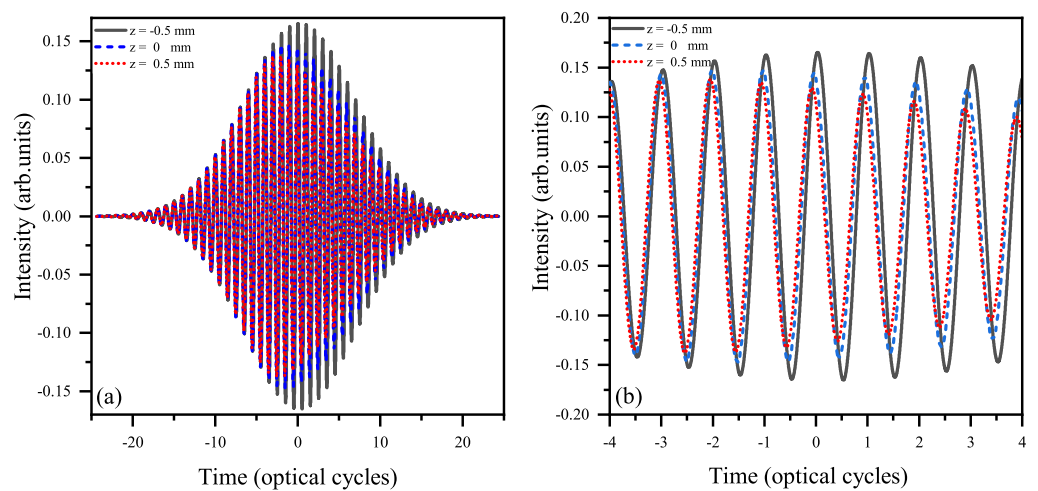


Figure 4. (a) Evolution of electricfield with time at different propagation locations; (b) partially enlarged details of (a).

We perform the Fourier transform in the time-domain electric field at various spatial locations to produce the frequency spectrum of the laser field, as shown in Figure 5, which allows us to examine the impact of this portion of frequency shift. It can be seen from Figure 5 that the fundamental frequency driving laser field at different spatial positions shows different characteristics, no matter whether $r = 0 \mu\text{m}$ (Figure 5a) or $r = 10 \mu\text{m}$ (Figure 5b): firstly, the spectrum intensity of the spectrum decreases rapidly with the increase in the propagation distance; secondly, the rate of decrease becomes more negligible beyond $z = 0 \text{ mm}$; thirdly, the spectrum peak also moves toward the high-energy zone; and finally, the frequency almost stops moving when it exceeds $z = 0 \text{ mm}$. The single-atom response changes when the laser field changes, and we then looked more closely at this variation.

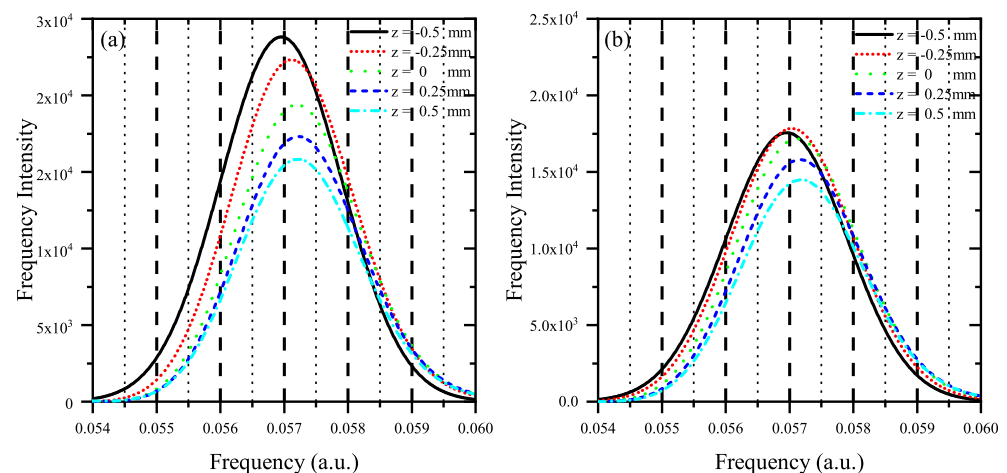


Figure 5. Variation of laser frequency amplitude with frequency at different propagation positions (a) $r = 0 \mu\text{m}$, (b) $r = 10 \mu\text{m}$

Figure 6 shows how the single-atom harmonic spectrum changes at $z = -0.5 \text{ mm}$, 0 mm , and 0.5 mm at a distance from the optical axis $r = 4 \mu\text{m}$. The harmonic emission spectrum in Figure 6a shows a fairly intricate structure at $z = -0.5 \text{ mm}$. In addition to the interference peaks caused by the driving laser envelope effect, odd harmonics can be observed in the harmonic spectrum, resulting from the driving laser's pulsing effect. It seems that the odd harmonic is still very near to the harmonic emission peak overall. However, the peak energy of the harmonic emission spectrum has shifted towards the high-energy area as due to the expanding propagation distance. Peak shift behavior can be seen in the harmonic emission spectra approaches at $z = 0 \text{ mm}$ (Figure 6b) and $z = 0.5 \text{ mm}$ (Figure 6c), which is consistent with the behavior of the driving laser field, where the high-intensity driving laser rapidly ionizes the gas target to produce plasma, causing a decrease in optical field strength and an increase in frequency as the propagation distance increases, resulting in a new frequency peak in the generated harmonic spectrum.

The above analysis reveals that the interaction of the high-intensity driving laser with the gas target changes the behavior of the driving laser field due to the scattering effect of the generated plasma, which further affects the change of the harmonic emission spectrum, resulting in the enhancement of the harmonic emission at certain frequencies. The density and laser parameters of the gas medium can be macroscopically changed to obtain harmonic enhancement for particular energies. In response, we examined how the gas pressure and the position of the gas target that interacts with the beam affect harmonic amplification. For gas target pressures of 20, 30, 40, and 50 torr, Figure 7a depicts the changes in harmonic emission intensity with harmonic order. As can be observed from the figure, when the gas pressure is low, harmonic intensity augments as the gas pressure rises. However, the gradual transition of the harmonic emission spectrum from a bimodal to a unimodal structure results in a decrease in the intensity of the odd harmonic peak relative to

the harmonic peak produced by the laser field change, which makes this feature all the more important because it allows for the modulation of shining efficiency at the corresponding frequency. Additionally, it is acknowledged that the new frequency's peak energy varies significantly under various pressure conditions. This approach may be utilized to produce the best modulation of the harmonic energy emitted. As illustrated in Figure 7b, we also looked into how the harmonic emission spectra changed as the focusing position changed. The relative strength of the harmonic peaks is altered by shifting the focusing location, as can be seen in Figure 7b; however, the overall efficiency of the harmonics is not much impacted. The odd harmonic of the input driving laser is still more noticeable when the gas target is in front of the laser focus. Nevertheless, the new frequency peak will be much higher than the odd harmonic peak produced by the input driving laser for the gas target behind the laser focus (marked by the blue dotted line in Figure 7b). Therefore, it is possible to control the effectiveness of the particular energy harmonics by the location of the driving laser interaction with the gas target without affecting the gas pressure or the driving laser's characteristics.

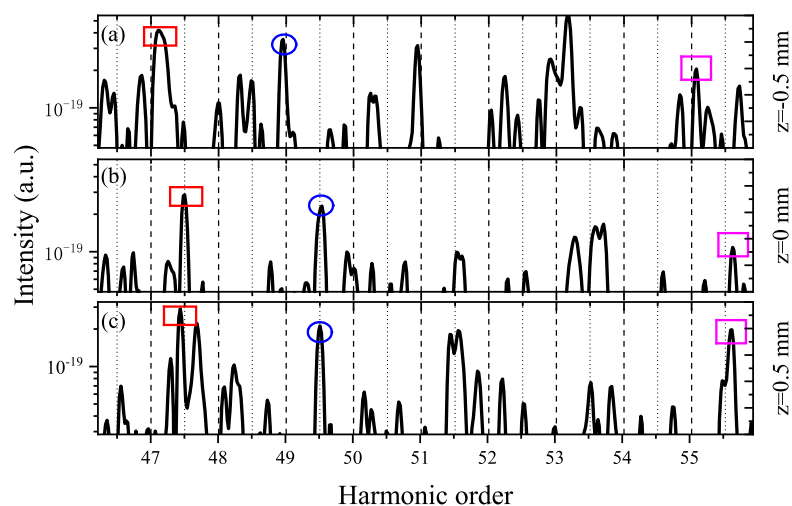


Figure 6. The harmonic spectra of single-atom response at $r = 4 \mu\text{m}$ for propagation positions of (a) $z = -0.5 \text{ mm}$, (b) $z = 0 \text{ mm}$, and (c) $z = 0.5 \text{ mm}$.

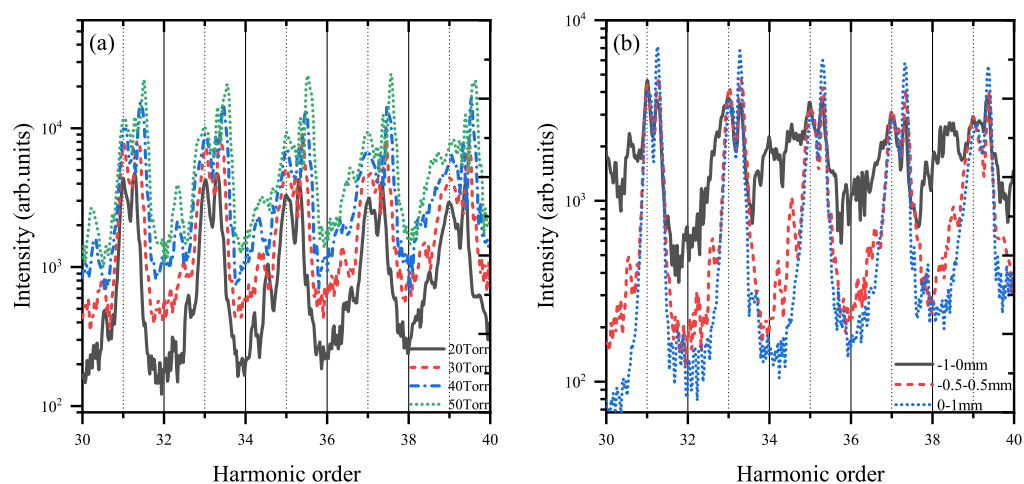


Figure 7. Macroscopic high-order harmonic spectra of 800 nm NIR laser pulses simulated by varying the focal length and pressure. (a) Harmonic spectra at different pressures on the gas target position of $-0.5\text{--}0.5 \text{ mm}$; (b) harmonic spectra at different focal lengths of the air pressure on 20 Torr.

To further regulate the efficiency and frequency of HHG, we increased the length of the laser pulse acting with the gas, while illustrating how harmonic intensity varies with propagation location, Figure 8 indicates how more atoms congregate, the medium enlarges, and the high-energy peaks become stronger as the propagation distance rises. Additionally, the number of peaks is growing and they are becoming larger and wider. Correspondingly, the harmonic efficiency is improving. Furthermore, it can be observed that the phenomena of multiple peaks occur at $z = 2.5$ mm, which might help us optimize the choice of a certain number of harmonics.

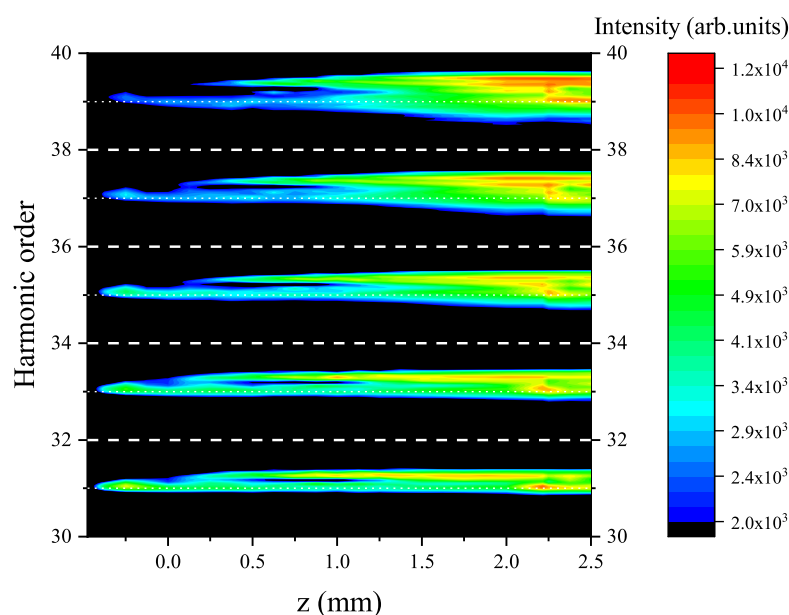


Figure 8. The harmonic emission spectrum at the propagation distance of 3 mm changing with the propagation position.

4. Conclusions

In this study, a theoretical analysis of the HHG of the Ne atom by a high-intensity laser is proposed. It has been discovered that the low-energy plateau of the harmonic emission spectrum has a double-peak structure. The laser field's analysis reveals that the intensity of the laser field falls as the propagation distance rises. The defocusing action of the plasma produced by the driving laser causes the frequency blue shift. New frequency harmonic peaks are formed by the changing the laser field. The effect of the gas target density, and the position of the gas target interaction with the laser pulses on this phenomenon was further examined. Our scheme could be employed to optimize the particular energy harmonics designed to improve the harmonic emission intensity.

Author Contributions: S.W.: data curation, writing—original draft and editing, and software. Y.P.: software. Y.Q.: supervision and editing. S.Z.: supervision and editing. H.Y.: software. J.W.: supervision and editing. F.G.: supervision. Y.Y.: editing, conceptualization, and supervision. All authors have read and agreed to the published version of the manuscript.

Funding: This research was funded by the National Key Research and Development Program of China (Grant Nos. 2019YFA0307700, 2022YFE0134200), National Natural Science Foundation of China (NSFC) (Grant Nos. 12074145, 12204214 and 11627807), Jilin Provincial Research Foundation for Basic Research, China (20220101003JC), and the Foundation of Education Department of Liaoning Province, China (LJKMZ20221435).

Institutional Review Board Statement: Not applicable.

Informed Consent Statement: Not applicable.

Data Availability Statement: The data presented in this study are available on request from the corresponding author.

Acknowledgments: We acknowledge both the High Performance Computing Center of Jilin University for the supercomputer time and the high performance computing cluster Tiger@ IAMP.

Conflicts of Interest: The authors declare no conflict of interest.

References

1. Tian, Y.Y.; Li, S.Y.; Wei, S.S.; Guo, F.M.; Zeng, S.L.; Chen, J.G.; Yang, Y.J. Investigation on the influence of atomic potentials on the above threshold ionization. *Chin. Phys. B* **2014**, *23*, 053202. [[CrossRef](#)]
2. Chen, J.; Luan, Z.; Zhou, Q.; Alzahrani, A.K.; Biswas, A.; Liu, W. Periodic soliton interactions for higher-order nonlinear Schrödinger equation in optical fibers. *Nonlinear Dyn.* **2020**, *100*, 2817–2821. [[CrossRef](#)]
3. Chen, J.; Liu, M.; Liu, X.; Ouyang, Y.; Liu, W.; Wei, Z. The SnS₂ SA with high modulation depth for passively Q-switched fiber laser. *Nanophotonics* **2020**, *9*, 2549–2555. [[CrossRef](#)]
4. Yuan, H.; Yang, Y.; Guo, F.; Wang, J.; Cui, Z. Influence of multiphoton resonance excitation on the above-threshold ionization of a hydrogen atom. *Opt. Express* **2022**, *30*, 19745–19756. [[CrossRef](#)]
5. Yan, J.Z.; Zhao, S.S.; Lan, W.D.; Li, S.Y.; Zhou, S.S.; Chen, J.G.; Zhang, J.Y.; Yang, Y.J. Calculation of high-order harmonic generation of atoms and molecules by combining time series prediction and neural networks. *Opt. Express* **2022**, *30*, 35444–35456. [[CrossRef](#)]
6. Yang, Y.J.; Chen, J.G.; Chi, F.P.; Zhu, Q.R.; Zhang, H.X.; Sun, J.Z. Ultrahigh harmonic generation from an atom with superposition of ground state and highly excited states. *Chin. Phys. Lett.* **2007**, *24*, 1537–1540.
7. Harris, S.; Macklin, J.; Hänsch, T. Atomic scale temporal structure inherent to high-order harmonic generation. *Opt. Commun.* **1993**, *100*, 487–490. [[CrossRef](#)]
8. Minemoto, S.; Umegaki, T.; Oguchi, Y.; Morishita, T.; Le, A.T.; Watanabe, S.; Sakai, H. Retrieving photorecombination cross sections of atoms from high-order harmonic spectra. *Phys. Rev. A* **2008**, *78*, 061402. [[CrossRef](#)]
9. Baggesen, J.C.; Madsen, L.B. On the dipole, velocity and acceleration forms in high-order harmonic generation from a single atom or molecule. *J. Phys. B At. Mol. Opt. Phys.* **2011**, *44*, 115601. [[CrossRef](#)]
10. Yu-Jun, Y.; Gao, C.; Ji-Gen, C.; Qi-Ren, Z. A time-distinguished analysis of the harmonic structure from a model molecular ion. *Chin. Phys. Lett.* **2004**, *21*, 652. [[CrossRef](#)]
11. Qiao, Y.; Wu, D.; Chen, J.G.; Wang, J.; Guo, F.M.; Yang, Y.J. High-order harmonic generation from H²⁺ irradiated by a co-rotating two-color circularly polarized laser field. *Phys. Rev. A* **2019**, *100*, 063428. [[CrossRef](#)]
12. Torres, R.; Kajumba, N.; Underwood, J.G.; Robinson, J.; Baker, S.; Tisch, J.; De Nalda, R.; Bryan, W.; Velotta, R.; Altucci, C.; et al. Probing orbital structure of polyatomic molecules by high-order harmonic generation. *Phys. Rev. Lett.* **2007**, *98*, 203007. [[CrossRef](#)]
13. Levesque, J.; Mairesse, Y.; Dudovich, N.; Pépin, H.; Kieffer, J.C.; Corkum, P.; Villeneuve, D. Polarization state of high-order harmonic emission from aligned molecules. *Phys. Rev. Lett.* **2007**, *99*, 243001. [[CrossRef](#)]
14. Qiao, Y.; Huo, Y.; Liang, H.; Chen, J.; Liu, W.; Yang, Y.; Jiang, S. Robust retrieval method of crystal transition dipole moments by high-order harmonic spectrum. *Phys. Rev. B* **2023**, *107*, 075201. [[CrossRef](#)]
15. Jiang, S.; Yu, C.; Chen, J.; Huang, Y.; Lu, R.; Lin, C. Smooth periodic gauge satisfying crystal symmetry and periodicity to study high-harmonic generation in solids. *Phys. Rev. B* **2020**, *102*, 155201. [[CrossRef](#)]
16. Qiao, Y.; Chen, J.; Huo, Y.; Liang, H.; Yu, R.; Yu, R.; Yang, Y. Effect of the interference between interband currents on the crystal harmonic spectra. *Phys. Rev. A* **2023**, *107*, 023523. [[CrossRef](#)]
17. Zhao, Y.; Xu, X.; Jiang, S.; Zhao, X.; Chen, J.; Yang, Y. Cooper minimum of high-order harmonic spectra from an MgO crystal in an ultrashort laser pulse. *Phys. Rev. A* **2020**, *101*, 033413. [[CrossRef](#)]
18. Zhao, Y.T.; Ma, S.y.; Jiang, S.C.; Yang, Y.J.; Zhao, X.; Chen, J.G. All-optical reconstruction of k-dependent transition dipole moment by solid harmonic spectra from ultrashort laser pulses. *Opt. Express* **2019**, *27*, 34392–34404. [[CrossRef](#)]
19. Qiao, Y.; Chen, J.; Chen, J. Review on the Reconstruction of Transition Dipole Moments by Solid Harmonic Spectrum. *Symmetry* **2022**, *14*, 2646. [[CrossRef](#)]
20. Qiao, Y.; Huo, Y.Q.; Jiang, S.C.; Yang, Y.J.; Chen, J.G. All-optical reconstruction of three-band transition dipole moments by the crystal harmonic spectrum from a two-color laser pulse. *Opt. Express* **2022**, *30*, 9971–9982. [[CrossRef](#)]
21. Krause, J.L.; Schafer, K.J.; Kulander, K.C. High-order harmonic generation from atoms and ions in the high intensity regime. *Phys. Rev. Lett.* **1992**, *68*, 3535. [[CrossRef](#)] [[PubMed](#)]
22. Paul, P.M.; Toma, E.S.; Breger, P.; Mullot, G.; Augé, F.; Balcou, P.; Muller, H.G.; Agostini, P. Observation of a train of attosecond pulses from high harmonic generation. *Science* **2001**, *292*, 1689–1692. [[CrossRef](#)] [[PubMed](#)]
23. Pan, Y.; Guo, F.; Yang, Y.; Ding, D. Effect of laser intensity on quantum trajectories in the macroscopic high-order harmonic generation. *Chin. Phys. B* **2019**, *28*, 113201. [[CrossRef](#)]
24. Han, J.X.; Wang, J.; Qiao, Y.; Liu, A.H.; Guo, F.M.; Yang, Y.J. Significantly enhanced conversion efficiency of high-order harmonic generation by introducing chirped laser pulses into scheme of spatially inhomogeneous field. *Opt. Express* **2019**, *27*, 8768–8776. [[CrossRef](#)] [[PubMed](#)]

25. Czwartos, J.; Zaszczynska, A.; Nowak-Stepniowska, A.; Fok, T.; Budner, B.; Bartnik, A.; Wachulak, P.; Kołbuk, D.; Sajkiewicz, P.; Fiedorowicz, H. The novel approach to physico-chemical modification and cytocompatibility enhancement of fibrous polycaprolactone (PCL) scaffolds using soft X-ray/extreme ultraviolet (SXR/EUV) radiation and low-temperature, SXR/EUV induced, nitrogen and oxygen plasmas. *Appl. Surf. Sci.* **2022**, *606*, 154779. [[CrossRef](#)]
26. Attwood, D.T.; Naulleau, P.; Goldberg, K.A.; Tejnil, E.; Chang, C.; Beguiristain, R.; Batson, P.; Bokor, J.; Gullikson, E.M.; Koike, M.; et al. Tunable coherent radiation in the soft X-ray and extreme ultraviolet spectral regions. *IEEE J. Quantum Electron.* **1999**, *35*, 709–720. [[CrossRef](#)]
27. Rego, L.; Brooks, N.J.; Nguyen, Q.L.; Román, J.S.; Binnie, I.; Plaja, L.; Kapteyn, H.C.; Murnane, M.M.; Hernández-García, C. Necklace-structured high-harmonic generation for low-divergence, soft X-ray harmonic combs with tunable line spacing. *Sci. Adv.* **2022**, *8*, eabj7380. [[CrossRef](#)]
28. Fan, T.; Grychtol, P.; Knut, R.; Hernández-García, C.; Hickstein, D.D.; Zusin, D.; Gentry, C.; Dollar, F.J.; Mancuso, C.A.; Hogle, C.W.; et al. Bright circularly polarized soft X-ray high harmonics for X-ray magnetic circular dichroism. *Proc. Natl. Acad. Sci. USA* **2015**, *112*, 14206–14211. [[CrossRef](#)]
29. Chini, M.; Zhao, K.; Chang, Z. The generation, characterization and applications of broadband isolated attosecond pulses. *Nat. Photonics* **2014**, *8*, 178–186. [[CrossRef](#)]
30. Park, I.Y.; Kim, S.; Choi, J.; Lee, D.H.; Kim, Y.J.; Kling, M.F.; Stockman, M.I.; Kim, S.W. Plasmonic generation of ultrashort extreme-ultraviolet light pulses. *Nat. Photonics* **2011**, *5*, 677–681. [[CrossRef](#)]
31. Kim, S.; Jin, J.; Kim, Y.J.; Park, I.Y.; Kim, Y.; Kim, S.W. High-harmonic generation by resonant plasmon field enhancement. *Nature* **2008**, *453*, 757–760. [[CrossRef](#)]
32. Heslar, J.; Telnov, D.A.; Chu, S.I. Enhancement of VUV and EUV generation by field-controlled resonance structures of diatomic molecules. *Phys. Rev. A* **2016**, *93*, 063401. [[CrossRef](#)]
33. Rundquist, A.; Durfee III, C.G.; Chang, Z.; Herne, C.; Backus, S.; Murnane, M.M.; Kapteyn, H.C. Phase-matched generation of coherent soft X-rays. *Science* **1998**, *280*, 1412–1415. [[CrossRef](#)]
34. Zhou, S.S.; Lan, W.D.; Chen, J.G.; Wang, J.; Guo, F.M.; Yang, Y.J. High-order harmonic generation of 1-nonene under linearly polarized laser pulses. *Phys. Rev. A* **2022**, *106*, 023510. [[CrossRef](#)]
35. Jiang, S.; Dorfman, K. Detecting electronic coherences by time-domain high-harmonic spectroscopy. *Proc. Natl. Acad. Sci. USA* **2020**, *117*, 9776–9781. [[CrossRef](#)]
36. Zhou, S.S.; Yang, Y.J.; Yang, Y.; Suo, M.Y.; Li, D.Y.; Qiao, Y.; Yuan, H.Y.; Lan, W.D.; Hu, M.H. High-order harmonic generation of the cyclo[18]carbon molecule irradiated by circularly polarized laser pulse. *Chin. Phys. B* **2023**, *32*, 013201. [[CrossRef](#)]
37. Popmintchev, T.; Chen, M.C.; Popmintchev, D.; Arpin, P.; Brown, S.; Ališauskas, S.; Andriukaitis, G.; Balčiunas, T.; Mücke, O.D.; Pugzlys, A.; et al. Bright coherent ultrahigh harmonics in the keV X-ray regime from mid-infrared femtosecond lasers. *Science* **2012**, *336*, 1287–1291. [[CrossRef](#)]
38. Gaumnitz, T.; Jain, A.; Pertot, Y.; Huppert, M.; Jordan, I.; Ardana-Lamas, F.; Wörner, H.J. Streaking of 43-attosecond soft-X-ray pulses generated by a passively CEP-stable mid-infrared driver. *Opt. Express* **2017**, *25*, 27506–27518. [[CrossRef](#)]
39. Watanabe, S.; Kondo, K.; Nabekawa, Y.; Sagisaka, A.; Kobayashi, Y. Two-color phase control in tunneling ionization and harmonic generation by a strong laser field and its third harmonic. *Phys. Rev. Lett.* **1994**, *73*, 2692. [[CrossRef](#)]
40. Tong, X.M.; Chu, S.I. Generation of circularly polarized multiple high-order harmonic emission from two-color crossed laser beams. *Phys. Rev. A* **1998**, *58*, R2656. [[CrossRef](#)]
41. Lan, P.; Lu, P.; Cao, W.; Li, Y.; Wang, X. Attosecond ionization gating for isolated attosecond electron wave packet and broadband attosecond xuv pulses. *Phys. Rev. A* **2007**, *76*, 051801. [[CrossRef](#)]
42. Hong, W.; Li, Y.; Lu, P.; Lan, P.; Zhang, Q.; Wang, X. Control of quantum paths in the multicycle regime and efficient broadband attosecond pulse generation. *JOSA B* **2008**, *25*, 1684–1689. [[CrossRef](#)]
43. Luo, J.; Li, Y.; Wang, Z.; He, L.; Zhang, Q.; Lan, P.; Lu, P. Efficient supercontinuum generation by UV-assisted midinfrared plasmonic fields. *Phys. Rev. A* **2014**, *89*, 023405. [[CrossRef](#)]
44. Takahashi, E.J.; Kanai, T.; Ishikawa, K.L.; Nabekawa, Y.; Midorikawa, K. Coherent water window x ray by phase-matched high-order harmonic generation in neutral media. *Phys. Rev. Lett.* **2008**, *101*, 253901. [[CrossRef](#)] [[PubMed](#)]
45. Ma, X.; Zeng, P.; Zhou, H. Phase-matching quantum key distribution. *Phys. Rev. X* **2018**, *8*, 031043. [[CrossRef](#)]
46. Hareli, L.; Shoulga, G.; Bahabad, A. Phase matching and quasi-phase matching of high-order harmonic generation—A tutorial. *J. Phys. B At. Mol. Opt. Phys.* **2020**, *53*, 233001. [[CrossRef](#)]
47. Balcou, P.; Salieres, P.; L’Huillier, A.; Lewenstein, M. Generalized phase-matching conditions for high harmonics: The role of field-gradient forces. *Phys. Rev. A* **1997**, *55*, 3204. [[CrossRef](#)]
48. Jianxin, C.; Yuanqin, X.; Qin, Y. High Harmonic Generation in N^{-2} Using Intense fs Laser Pulses. *Acta Opt. Sin.* **2002**, *22*, 650–653.
49. Pan, Y.; Guo, F.; Jin, C.; Yang, Y.; Ding, D. Selection of electron quantum trajectories in the macroscopic high-order harmonics generated by near-infrared lasers. *Phys. Rev. A* **2019**, *99*, 033411. [[CrossRef](#)]
50. Wahlström, C.G.; Larsson, J.; Persson, A.; Starczewski, T.; Svanberg, S.; Salieres, P.; Balcou, P.; L’Huillier, A. High-order harmonic generation in rare gases with an intense short-pulse laser. *Phys. Rev. A* **1993**, *48*, 4709. [[CrossRef](#)]
51. Shin, H.J.; Lee, D.G.; Cha, Y.H.; Hong, K.H.; Nam, C.H. Generation of nonadiabatic blueshift of high harmonics in an intense femtosecond laser field. *Phys. Rev. Lett.* **1999**, *83*, 2544. [[CrossRef](#)]

52. Kan, C.; Capjack, C.; Rankin, R.; Burnett, N. Spectral and temporal structure in high harmonic emission from ionizing atomic gases. *Phys. Rev. A* **1995**, *52*, R4336. [[CrossRef](#)]
53. Altucci, C.; Bruzzese, R.; De Lisio, C.; Nisoli, M.; Stagira, S.; De Silvestri, S.; Svelto, O.; Boscolo, A.; Ceccherini, P.; Poletto, L.; et al. Tunable soft-x-ray radiation by high-order harmonic generation. *Phys. Rev. A* **1999**, *61*, 021801. [[CrossRef](#)]
54. Lu, F.M.; Xia, Y.Q.; Zhang, S.; Chen, D.Y. Investigation of tunable coherent XUV light source by high harmonics generation using intense femtosecond laser pulses in Ne. *Acta Phys. Sin* **2013**, *62*, 024212.
55. Reitze, D.H.; Kazamias, S.; Weihe, F.; Mullot, G.; Douillet, D.; Augé, F.; Albert, O.; Ramanathan, V.; Chambaret, J.P.; Hulin, D.; et al. Enhancement of high-order harmonic generation at tuned wavelengths through adaptive control. *Opt. Lett.* **2004**, *29*, 86–88. [[CrossRef](#)]
56. Nefedova, V.; Ciappina, M.; Finke, O.; Albrecht, M.; Vábek, J.; Kozlová, M.; Suárez, N.; Pisanty, E.; Lewenstein, M.; Nejd, J. Determination of the spectral variation origin in high-order harmonic generation in noble gases. *Phys. Rev. A* **2018**, *98*, 033414. [[CrossRef](#)]
57. Lewenstein, M.; Balcou, P.; Ivanov, M.Y.; L’huillier, A.; Corkum, P.B. Theory of high-harmonic generation by low-frequency laser fields. *Phys. Rev. A* **1994**, *49*, 2117. [[CrossRef](#)]
58. Esarey, E.; Sprangle, P.; Krall, J.; Ting, A. Self-focusing and guiding of short laser pulses in ionizing gases and plasmas. *IEEE J. Quantum Electron.* **1997**, *33*, 1879–1914. [[CrossRef](#)]
59. Takahashi, E.; Tosa, V.; Nabekawa, Y.; Midorikawa, K. Experimental and theoretical analyses of a correlation between pump-pulse propagation and harmonic yield in a long-interaction medium. *Phys. Rev. A* **2003**, *68*, 023808. [[CrossRef](#)]
60. Geissler, M.; Tempea, G.; Scrinzi, A.; Schnürer, M.; Krausz, F.; Brabec, T. Light propagation in field-ionizing media: Extreme nonlinear optics. *Phys. Rev. Lett.* **1999**, *83*, 2930. [[CrossRef](#)]
61. Siegman, A. Lasers (University Science, Mill Valley, CA, 1986). *Chap* **1991**, *29*, 1129–1170.
62. L’Huillier, A.; Balcou, P.; Candel, S.; Schafer, K.J.; Kulander, K.C. Calculations of high-order harmonic-generation processes in xenon at 1064 nm. *Phys. Rev. A* **1992**, *46*, 2778. [[CrossRef](#)] [[PubMed](#)]
63. Tosa, V.; Kim, K.T.; Nam, C.H. Macroscopic generation of attosecond-pulse trains in strongly ionized media. *Phys. Rev. A* **2009**, *79*, 043828. [[CrossRef](#)]
64. Shang, B.; Qi, P.; Guo, J.; Zhang, Z.; Guo, L.; Chu, C.; Liu, J.; Kosareva, O.G.; Zhang, N.; Lin, L.; et al. Manipulation of Long-Distance femtosecond laser Filamentation: From physical model to acoustic diagnosis. *Opt. Laser Technol.* **2023**, *157*, 108636. [[CrossRef](#)]
65. Guo, H.; Wang, T.J.; Zhang, X.; Liu, C.; Chen, N.; Liu, Y.; Sun, H.; Shen, B.; Jin, Y.; Leng, Y.; et al. Direct measurement of radial fluence distribution inside a femtosecond laser filament core. *Opt. Express* **2020**, *28*, 15529–15541. [[CrossRef](#)]
66. Zheng, H.; Yin, F.; Wang, T.J.; Liu, Y.; Wei, Y.; Zhu, B.; Zhou, K.; Leng, Y. Time-resolved measurements of electron density and plasma diameter of 1 kHz femtosecond laser filament in air. *Chin. Opt. Lett.* **2022**, *20*, 093201. [[CrossRef](#)]
67. Major, B.; Kovács, K.; Svirplys, E.; Anus, M.; Ghafur, O.; Varjú, K.; Vrakking, M.; Tosa, V.; Schütte, B. High-harmonic generation in a strongly overdriven regime. *arXiv* **2022**, arXiv:2203.11021.
68. Jin, C.; Chen, M.C.; Sun, H.W.; Lin, C. Extension of water-window harmonic cutoff by laser defocusing-assisted phase matching. *Opt. Lett.* **2018**, *43*, 4433–4436. [[CrossRef](#)]
69. Csizmadia, T.; Oldal, L.G.; Ye, P.; Majorosi, S.; Tzallas, P.; Sansone, G.; Tosa, V.; Varjú, K.; Major, B.; Kahaly, S. Detailed study of quantum path interferences in high harmonic generation driven by chirped laser pulses. *New J. Phys.* **2021**, *23*, 123012. [[CrossRef](#)]

Disclaimer/Publisher’s Note: The statements, opinions and data contained in all publications are solely those of the individual author(s) and contributor(s) and not of MDPI and/or the editor(s). MDPI and/or the editor(s) disclaim responsibility for any injury to people or property resulting from any ideas, methods, instructions or products referred to in the content.